Physics Letters A 379 (2015) 3008–3012

Contents lists available at ScienceDirect

Physics Letters A

www.elsevier.com/locate/pla

Design and analyses of an ultra-thin flat lens for wave front shaping in the visible

Kai Huang [a], Yiyan Li [b], Xuelong Tian [a,*], Dajun Zeng [a], Xueli Gao [a]

[a] Department of Biomedical Engineering, Bioengineering College of Chongqing University, Chongqing University, Chongqing 400044, China
[b] Department of Electrical and Computer Engineering, University of Nevada, Las Vegas, Las Vegas, NV 89154-4026, USA

ARTICLE INFO

Article history:
Received 21 April 2015
Received in revised form 1 August 2015
Accepted 2 August 2015
Available online 21 August 2015
Communicated by R. Wu

Keywords:
Moment method
Focal plane
Nanoantenna
Phase discontinuities
Snell's law

ABSTRACT

An ultra-thin flat lens is proposed for focusing circularly polarized light in the visible range. Anisotropic C-shaped nanoantennas with phase discontinuities are used to form the metasurface of the lens. The phase response of the C-shaped nanoantennas can be manipulated by simply rotating the angle of the unit nanoantenna. A 600 nm incident circularly polarized light is focused by the proposed techniques. Good agreements are observed by using our MoM and a commercial FDTD software package. The computation time spent by using MoM is approximately 10–100 times smaller than using FDTD. All the results show the proposed nanoantenna array has a great potential for nanoscale optical microscopy, solar cell energy conversion enhancement, as well as integrated optical circuits.

1. Introduction

Differently from the gradual phase changes along the optical path in traditional bulk lenses, prisms and gratings, nanoantenna-based metasurfaces can create abrupt phase shifts in the wavelength scale [1]. The greatest benefit of using this technique is in making highly customizable and scalable lenses with large aperture and short focal length [1]. The potential applications are numerous, for example, embedded light-on-a-chip system [2], super-resolution imaging [3], nanolithography [4] and broadband chromatic optical systems [5]. Recently, different topologies of the non-uniform metamaterial units have been investigated, such as V-shaped anisotropic dipoles [1–4,6], phase-conjugated dipole rod [6] and variant widths (or depths) nano-slits [7]. Additionally, traditional log-periodic antennas have been redesigned in nanoscale to obtain broadband resonance in terahertz incident levels [8].

An alternative topology proposed here is a C-shaped nanoantenna [9] for focusing the light in the visible range. C-shaped nanoantennas have several advantages in phase manipulation over other nanoantenna topologies. The phase discontinuity manipulation of the C-shaped nanoantenna can simply be implemented by rotating the angle of the body which improves the cross-polarization ratio by using this geometry. A 2-D phased array of the C-shaped nanoantennas are designed and numerically analyzed in this study.

To customize the parameters such as the focal length, beam width and phase distribution of the C-shaped nanoantenna based metasurfaces, numerical simulations such as finite-difference time-domain (FDTD) and moment method (MoM) are conducted to provide guidance for the future nano-fabrication. Due to the increasing scale of the nanoantenna array, the simulation usually takes a couple of days or even several weeks using FDTD [10]. The MoM particularly designed for the proposed nanoantenna array in this study effectively shortens the simulation time without losing significant resolution. Anomalous refraction and focus properties are investigated by our MoM and FDTD in both time and frequency domain. Results show good agreements between our MoM and a FDTD software package.

2. Materials and methods

Fig. 1 shows the nanoantenna array designed in this study. A C-shaped nanoantenna is used as the unit cell for the array. The C-shaped nanoantenna with a rotation angle of θ is shown in Fig. 1. The rotation angle θ is the angle between the localized optical axis of the unit C-shaped nanoantenna and the horizontal axis in the clockwise direction (Fig. 2(b)). The dimension of the nanoantenna is designed as $\lambda = 2.21a$, $b = 0.6a$, $c = 0.2a$ [9]. Wavelength

* Corresponding author at: Chongqing University, Department of Biomedical Engineering, 174 Shazhengjie, Shapingba, Chongqing 400044, China. Tel.: +86 13060251869.
E-mail addresses: nianhua110@hotmail.com (K. Huang), liy10@unlv.nevada.edu (Y. Li), xltian@cqu.edu.cn (X. Tian), dajunzeng@163.com (D. Zeng), 2455031293@qq.com (X. Gao).

http://dx.doi.org/10.1016/j.physleta.2015.08.022
0375-9601/

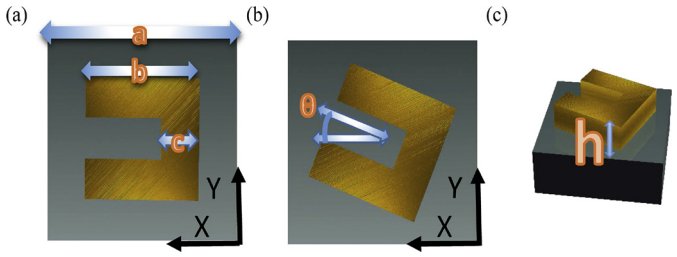

Fig. 1. The geometric parameters of the unit C-shaped nanoantenna. 'a' is the width of the unit cell. 'b', 'c' and 'h' are the length, width and height of each nanoantenna. 'θ' is the rotation angle of the C-shaped nanoantenna.

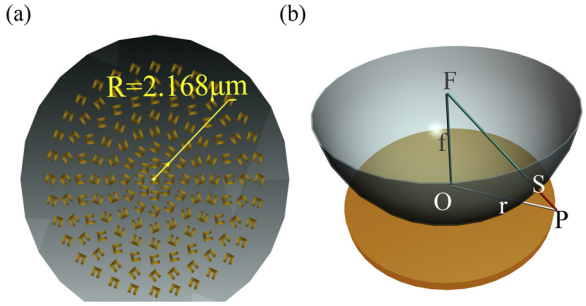

Fig. 2. (a) The schematic of the two-dimensional circular array. (b) The parabolic phase profile of the scattering light. 'P' is a point on the metasurface. 'S' is the projection of point 'P' onto the parabolic surface. 'O' is the center of the circular lens. The length of PS is proportional to the length of PO.

λ is 600 nm. $a = 271$ nm, $b = 163$ nm, $c = 54$ nm. The incident light is left circularly polarized.

The relationship between the phase profile of the nanoantennas Φ and its location center coordinate x is shown in Eq. (1) [9,11,12]:

$$n_t \sin\alpha_t - n_i \sin\alpha_i = \frac{\lambda}{2\pi}\frac{d\Phi}{dx} \tag{1}$$

where n_t is the refractive index of the medium where the light is leaving, n_i is the refractive index of the medium where the light is entering. α_t and α_i are the angle between the corresponding light and the normal to the medium interface. If $\alpha_t = 0$ and substituting $\Phi = 2\theta = 2k\pi x = \frac{2k_g\pi}{a}x$ into Eq. (2), the angle of refraction for the scattering cross-polarized beam is obtained as:

$$\alpha_t = \arcsin\left(-\frac{\lambda}{2\pi}\times\frac{d\Phi}{dx}\right) = \arcsin(-2.21k_g) \tag{2}$$

where k_g is the gradient of the phase variation. Then we get:

$$\Phi(x) = 2\theta = 2k\pi x = -\frac{2\pi\sin(\alpha_t)}{2.21a} \tag{3}$$

In order to provide a parabolic wave front, the phase shift in every unit is described by Eq. (4) [9,13]. In Eq. (4), f_d is the given focal length, λ is wavelength, x and y is the coordination of the nanoantenna unit. Φ is the phase shift in every unit nanoantenna. The phase profile is plotted in Fig. 2(b). With fixed focus length f_d and incident wavelength λ, the scattering phase is distributed concentrically along the radius of the plate:

$$\Phi(x,y) = \frac{2\pi f_d}{\lambda} - \frac{2\pi\sqrt{f_d^2 + x^2 + y^2}}{\lambda} \tag{4}$$

The lens is divided into 'm' annular areas concentrically. The nanoantenna units in each annular area have the same geometry, orientation angle and phase shifts to the incident light [14]. For a given focus length f_d, the coordinate and the phase shift φ of each unit must satisfy Eq. (5) [14]:

$$\begin{cases} x_{i,j} = i\times a\times\cos\left(\dfrac{2\pi}{n}\times j\right) \\ y_{i,j} = i\times a\times\cos\left(\dfrac{2\pi}{n}\times j\right) \\ \varphi_{i,j} = \dfrac{2\pi f_d}{\lambda} - \dfrac{2\pi\sqrt{f_d^2 + (i\times a)^2}}{\lambda} \end{cases} \tag{5}$$

$i = 0,\ldots,m$, $j = 1,\ldots,n$, where 'i' means the i-th annulus ($i = 0$ corresponds to the center nanoantenna). 'j' means the j-th nanoantenna in the i-th annulus. 'a' is the width of every annulus. Fig. 2(a) shows the schematic of the 2-D circularly arranged lens.

The MoM uses the triangular-type "rooftop" vector basis functions to represent the surface-induced current. The PDE tools of MATLAB were used to create the triangle meshes. In the MoM, surface-induced current must be solved by linear equations (Eq. (6)) [15], where V is the voltage matrix, Z is the impedance matrix, and I is the unknown current matrix:

$$V = Z\cdot I \tag{6}$$

The voltage elements V_m and the impedance elements Z_{mn} are given by Eq. (7) and Eq. (8):

$$V_m = l_m\left(E_m^+\cdot\frac{\rho_m^{c+}}{2} + E_m^-\cdot\frac{\rho_m^{c-}}{2}\right) \tag{7}$$

$$Z_{mn} = l_m j\omega\left(A_{mn}^+\cdot\frac{\rho_m^{c+}}{2} + A_{mn}^-\cdot\frac{\rho_m^{c-}}{2} + \Phi_{mn}^- - \Phi_{mn}^+\right) \tag{8}$$

where

$$A_{mn}^{\pm} = \frac{\mu}{4\pi}\int_S \boldsymbol{f_n}(\boldsymbol{r}')\frac{e^{-jkR_m^{\pm}}}{R_m^{\pm}}dS' \tag{9}$$

$$\Phi_{mn}^{\pm} = -\frac{1}{4\pi j\omega\varepsilon}\int_S \nabla_s'\cdot\boldsymbol{f_n}(\boldsymbol{r}')\frac{e^{-jkR_m^{\pm}}}{R_m^{\pm}}dS' \tag{10}$$

$$\boldsymbol{E_m^{\pm}} = \boldsymbol{E^i}(\boldsymbol{r_m^{c\pm}}) \tag{11}$$

$$R_m^{\pm} = \left|\boldsymbol{r_m^{c\pm}} - \boldsymbol{r}'\right| \tag{12}$$

$\boldsymbol{f_n}(\boldsymbol{r})$ is the basis function for MoM, $R_m^{\pm}$ represents the distance from any point $\boldsymbol{r}$ to the midpoint of edge $\boldsymbol{m}$. $\boldsymbol{E^i}(\boldsymbol{r_m^{c\pm}})$ represents the incident electric field at a point $\boldsymbol{r_m^{c\pm}}$:

$$\boldsymbol{f_n}(\boldsymbol{r}) = \begin{cases} \frac{l_n}{2A_n^+}\rho_n^+, & \boldsymbol{r}\text{ in }T_n^+ \\ \frac{l_n}{2A_n^-}\rho_n^-, & \boldsymbol{r}\text{ in }T_n^- \\ 0, & \text{otherwise} \end{cases} \tag{13}$$

l_n is the length of the edge of the triangle pair $T_n^{\pm}$. $A_n^{\pm}$ is the area of the triangle pair $T_n^{\pm}$.

The results obtained from our MoM are completed to a FDTD solution software package (FDTD Solutions, Lumerical Solutions Inc., Vancouver, Canada). 'Total field scattering field source' was used as the incident light. FDTD is a direct solution of Maxwell's time dependent curl equations. FDTD uses central-difference to approximate the space and time derivatives to avoid solving huge matrices for frequency-domain integral-equations and requires no calculation of structure-dependent Green functions [16]. The FDTD simulation dimension in this study is 4.2 μm in the X direction, 0.4 μm in the Y direction and 0.2 μm in the Z direction. A Perfectly matched layer absorbing boundary condition, containing 64 layers, is adopted in all directions. The condition of convergence is less than 10^{-5}. The mesh length in X and Y directions are set as 5 nm. Length in the Z direction is varying.

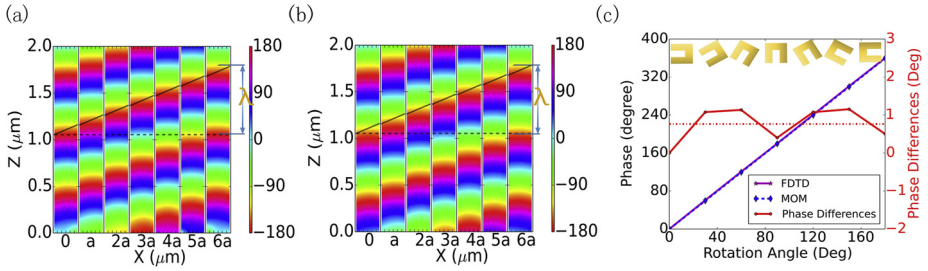

Fig. 3. Phase distributions of the scattering light calculated by the MoM (a) and FDTD (b). (c) Diagram of the phases of the scattering light at 1.2 μm along the Z axis.

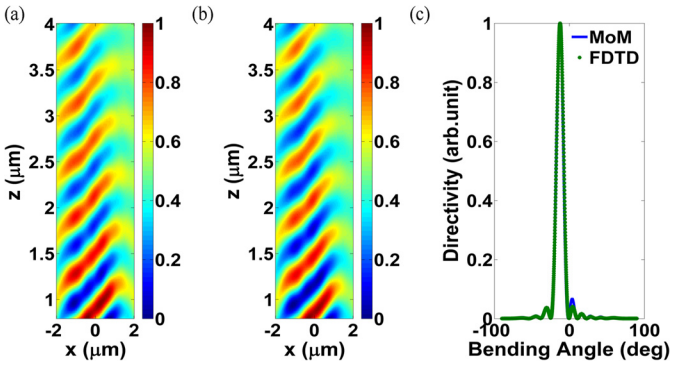

Fig. 4. The distribution of the electric field X component calculated by MoM (a) and FDTD (b). (c) The radiation pattern calculated by MoM (solid blue line) and FDTD (dashed green line). (For interpretation of the references to color in this figure, the reader is referred to the web version of this article.)

3. Results and discussion

All the simulations are implemented on a workstation (CPU: Intel Core i7-4790K 3.4 GHz; RAM: Kingston DDR3 32 GB; Harde Driver: Seagate ST1000DM003 1TB). Fig. 3 shows the phase responses of the unit cells with different rotation angles under the 600 nm left circularly polarized incident light. FDTD (Fig. 3(a)) and MoM (Fig. 3(b)) are used to obtain the space phase distributions. Fig. 3(c) shows the phases calculated by the two methods. The phase distribution calculated by the two methods are pretty close to each other, so we use the red solid line to show the subtle phase differences. The red dashed horizontal line is the average value of the differences which is 0.76 degree.

The nanoantenna array has 11 gradual phase shifts in 2.981 μm for the linear phase variation from 0 to 2π. For example, if the rotation angle θ is 0.1π, the bending angle can be obtained by Eq. (14). The bending angles are $\alpha_{t,MOM} = -12.56°$ (by MoM) and $\alpha_{t,FDTD} = -12.38°$ (by FDTD), which are close to the result obtained from Eq. (14) ($-12.7°$):

$$\alpha_t = \arsin\left(-\frac{2.21 * 0.1\pi}{\pi}\right) = -12.7 \tag{14}$$

The far field directivity is calculated by MoM and FDTD (Fig. 4c). Good agreements are found between the two methods in calculating the time-domain intensity profile and the far-field directivity.

The radius of the circular nanoantenna array is 2.168 μm. Fig. 5 shows the focusing beam properties calculated by MoM (Fig. 5(a)) and FDTD (Fig. 5(b)). The focus length is 2.261 μm by MoM and 2.234 μm by FDTD respectively. The difference of the focus length calculated by the two methods is 0.027 μm. The FWMH is 0.469 μm by MoM and 0.465 μm by FDTD. The difference between the results calculated by the two methods is less than 0.0004 μm.

Fig. 6 shows the variations of the focus length, FWHM and DOF with various f_d values. Good agreements are found by using the two computational methods.

Numerical simulations such as MoM and FDTD shown in this study provide an intuitive way to understand the scattering electric field distributions in space. Results show the parameters obtained by the MoM are close to the results obtained by FDTD. In MoM modeling, the scattering object is treated as a dipole array; the near-field intensity and phase distribution are more likely influenced by the interaction among the dipoles than the far-field intensity and phase distribution [17]. So the near-field simulations of the two methods have more deviations. The deviations become negligible if the focal length satisfies Eq. (15):

$$f > \frac{2D^2}{\lambda} \tag{15}$$

where f is the focus length, D is the effective length of the nanoantenna, λ is the wavelength of the incident light.

The accuracy of MoM depends on the mesh density, the number of mesh defects and the geometrical discretization error [16,18]. We assume that the increase in the number of meshes can improve the accuracy of the simulation. Fig. 7 shows when the number of triangles in a unit increases from 100 to 700, the accuracy increases by 0.02 μm (compared to the theoretical calculation), but the time spent on the simulation exponentially increases significantly. When the number of triangles in a unit is larger than 500, the focus length calculated by MoM is 2.171 μm, which is close to the result calculated by FDTD (2.173 μm).

In FDTD, influences of varied nanoantenna unit length and width on simulation time and focus length are evaluated. Simulation time increased dramatically when the dimension of the nanoantenna increased. The effectiveness of comparing the efficiency of FDTD and MoM may be argued when the dimension of the nanoantenna unit and the space grid density are modeled by different theories. But no matter how we shrank the size of the nanoantennas in FDTD, the time spent on FDTD was always at least 60 times longer than the time spent on MoM. But the electrical field profiles produced by the two methods are close. So MoM is more timely efficient in nanoantenna numerical computation in our study.

In Fig. 8, the mesh length in Z direction is set as 5 nm, length in other directions are varying. If the length and width of the mesh decreased to 6 nm, the focus length deviations to the theoretical value can be as low as 0.001 μm. But the time consumption increases dramatically, which is much larger than that in MoM.

C-shaped nanoantenna-based ultra-thin lenses are investigated by using FDTD and our MoM. The MoM can get a similar numerical result to FDTD in less time. The MoM enables a fast probing of the parameters of a nanoantenna-based ultra-thin lens. The MoM saves the computer resources and makes it possible to simulate a larger mesh grid without requiring too much memory space and computation time. FDTD is time-consuming when deriving the far-field light properties from solving the Cartesian Yee cells in space [15,16]. However, MoM [19] solves the excited current by directly solving electric field integral equations, which is much more time-efficient than FDTD which calculates the electric and magnetic field in every grid in the 3-D space. The most obvious advantage of

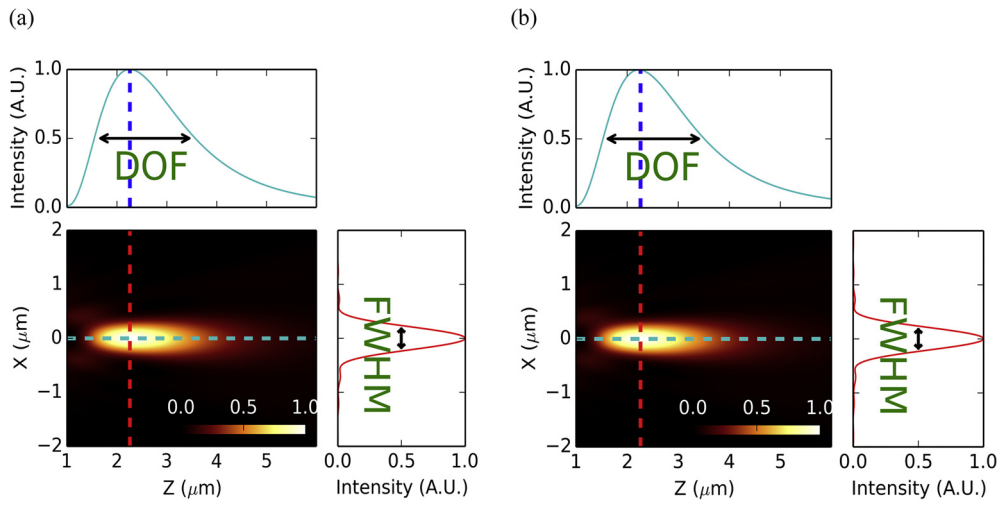

Fig. 5. Diagrams of the electric field intensity distributions calculated by MoM (a), FDTD (b).

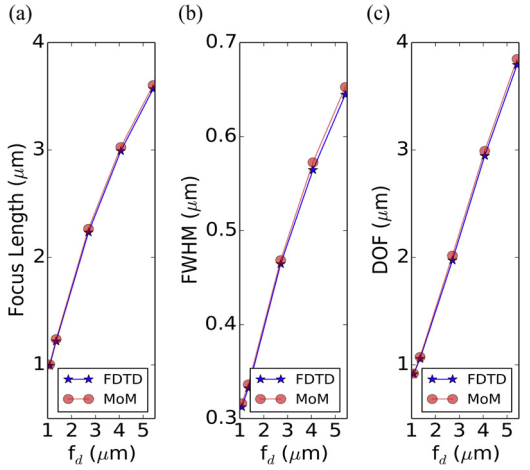

Fig. 6. Diagrams of the focal length (a), FWHM (b) and DOF (c) with various f_d.

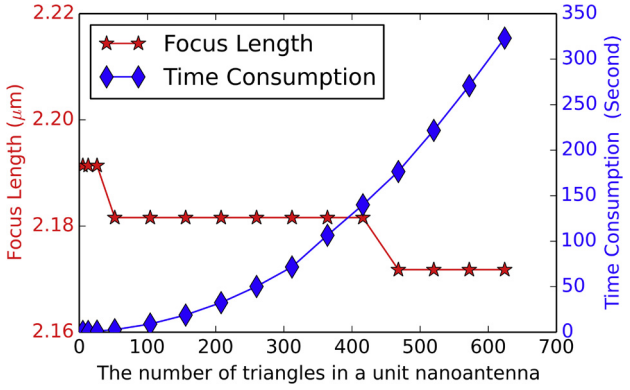

Fig. 7. The focus length calculated by MoM with varying amount of triangles in a unit cell. When the focus length f_d is 2.71 μm, the corresponding focus length obtained from FDTD is 2.173 μm.

our MoM grids over other rectangular patch grids is using triangular patches to approximate curly surface edges. Hence it is able to accurately model any geometry surface or boundary. Our MoM combines the advantages of triangular mesh modeling and the electric field integral equations (EFIE), which results in a set of simple and efficient algorithms. The essential parts of the algorithms are building the basis functions to represent the current

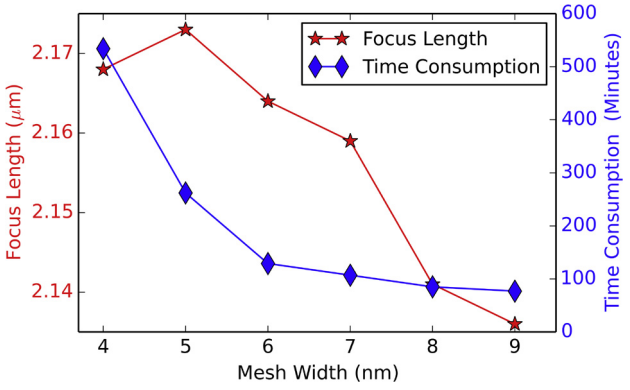

Fig. 8. The focus length calculated by FDTD with different mesh width.

density normal to the triangle edge elements. The basis function is a function of object mesh topologies, which won't be affected by incident waves. Therefore, MoM has a great potential to improve the simulation efficiency of large-scale nanoantenna metasurfaces.

Most metasurface studies focus on single frequency analyses [12,13,21,22]. Bandwidth limitation is the major problem of the current popular phased metasurface arrays, such as the 'V-shaped' nanoantenna arrays [22]. Wavelength dependent diffractive optical devices focus chromatic incident lights to different distances and cause major aberrations. Recently, eliminating the aberrations in broadband metasurface design has attracted lots of attention [5,23–25]. However, multi-band metasurface analyses introduces a tremendous amount of computation load. FDTD is a set of time-dependent iterations which is time consuming. Even powerful distributed computation workstations are helpless in improving the computation efficiency due to the iterative dependence. The MoM method proposed in this study is a good alternative for this type of time-dependent iterations.

To use the MoM method for broadband applications, the intensity distributions upon multi-frequencies are obtained by frequency sweeps. The nanoantenna mesh models should be updated for each step to match the various incident wavelengths [18]. Unknown surface-induced current 'I' can be solved by Eq. (1), where V is the voltage matrix, Z is the impedance matrix:

$$V = Z \cdot I \tag{1}$$

The algorithm flow chart is shown in Fig. 9.

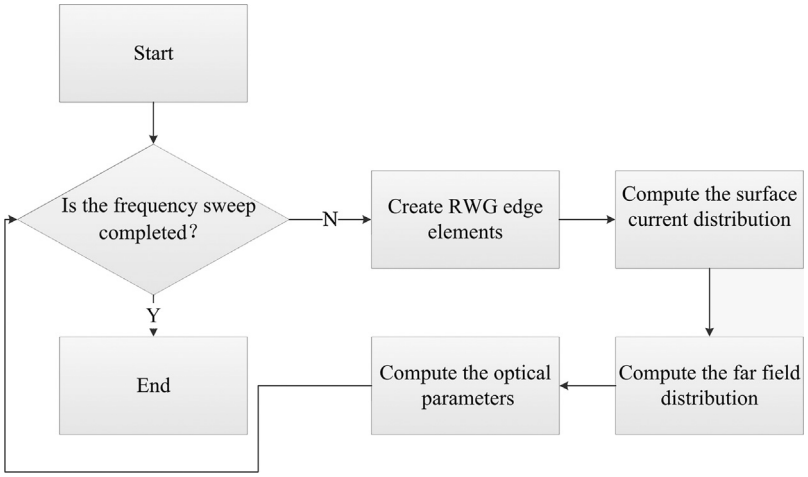

Fig. 9. The algorithm flow chart of the MoM method for multi-wavelength applications.

4. Conclusion

FDTD is one of the most popular tools for nanoantenna-based metasurface simulation [11,14,20]. In this study, FDTD is used to verify the validity of the numerical calculations done by MoM. Based upon the simulation results, the 2-D arranged nanoantenna array shows a good focus property at 600 nm. The far field electric field intensity, phase distribution and the directivity are calculated by both MoM and FDTD. Good agreements are observed between MoM and the FDTD software package but the MoM is apparently more efficient. The simulation results presented in this study provides important references for the 'C-shaped' lens fabrication and implicates the potential applications of MoM in both narrow-band and broadband nanoantenna computation.

Acknowledgements

The authors acknowledge helpful discussions with Dr. Jun Luo at Chongqing University.

References

[1] X. Ni, S. Ishii, A.V. Kildishev, V.M. Shalaev, Ultra-thin, planar, Babinet-inverted plasmonic metalenses, Light Sci. Appl. 2 (2013) e72, http://dx.doi.org/10.1038/lsa.2013.28.
[2] A. Reinhard, T. Volz, M. Winger, A. Badolato, K.J. Hennessy, E.L. Hu, et al., Strongly correlated photons on a chip, Nat. Photonics 6 (2012) 93–96, http://dx.doi.org/10.1038/nphoton.2011.321.
[3] B.D.F. Casse, W.T. Lu, Y.J. Huang, E. Gultepe, L. Menon, S. Sridhar, Super-resolution imaging using a three-dimensional metamaterials nanolens, Appl. Phys. Lett. 96 (2010) 023114, http://dx.doi.org/10.1063/1.3291677.
[4] A. Sundaramurthy, P.J. Schuck, N.R. Conley, D.P. Fromm, G.S. Kino, W.E. Moerner, Toward nanometer-scale optical photolithography: utilizing the near-field of bowtie optical nanoantennas, Nano Lett. 6 (2006) 355–360, http://dx.doi.org/10.1021/nl052322c.
[5] F. Aieta, M.A. Kats, P. Genevet, F. Capasso, Multiwavelength achromatic metasurfaces by dispersive phase compensation, Science 347 (2015) 1342–1345, http://dx.doi.org/10.1126/science.aaa2494.
[6] P.-Y. Chen, A. Alù, Subwavelength imaging using phase-conjugating nonlinear nanoantenna arrays, Nano Lett. 11 (2011) 5514–5518, http://dx.doi.org/10.1021/nl203354b.
[7] H. Shi, C. Wang, C. Du, X. Luo, X. Dong, H. Gao, Beam manipulating by metallic nano-slits with variant widths, Opt. Express 13 (2005) 6815, http://dx.doi.org/10.1364/OPEX.13.006815.
[8] D.M. Solís, J.M. Taboada, M.G. Araújo, F. Obelleiro, J.O. Rubiños-López, Design of optical wide-band log-periodic nanoantennas using surface integral equation techniques, Opt. Commun. 301–302 (2013) 61–66, http://dx.doi.org/10.1016/j.optcom.2013.03.047.
[9] M. Kang, T. Feng, H.-T. Wang, J. Li, Wave front engineering from an array of thin aperture antennas, Opt. Express 20 (2012) 15882–15890, http://dx.doi.org/10.1364/OE.20.015882.
[10] R. Blanchard, G. Aoust, P. Genevet, N. Yu, M.A. Kats, Z. Gaburro, et al., Modeling nanoscale V-shaped antennas for the design of optical phased arrays, Phys. Rev. B 85 (2012), http://dx.doi.org/10.1103/PhysRevB.85.155457.
[11] F. Aieta, P. Genevet, N. Yu, M.A. Kats, Z. Gaburro, F. Capasso, Out-of-plane reflection and refraction of light by anisotropic optical antenna metasurfaces with phase discontinuities, Nano Lett. 12 (2012) 1702–1706, http://dx.doi.org/10.1021/nl300204s.
[12] N. Yu, P. Genevet, M.A. Kats, F. Aieta, J.-P. Tetienne, F. Capasso, et al., Light propagation with phase discontinuities: generalized laws of reflection and refraction, Science 334 (2011) 333–337, http://dx.doi.org/10.1126/science.1210713.
[13] F. Aieta, A. Kabiri, P. Genevet, N. Yu, M.A. Kats, Z. Gaburro, et al., Reflection and refraction of light from metasurfaces with phase discontinuities, J. Nanophotonics 6 (2012) 063532, http://dx.doi.org/10.1117/1.JNP.6.063532.
[14] J. Lin, S. Wu, X. Li, C. Huang, X. Luo, Design and numerical analyses of ultrathin plasmonic lens for subwavelength focusing by phase discontinuities of nanoantenna arrays, Appl. Phys. Express 6 (2013) 022004, http://dx.doi.org/10.7567/APEX.6.022004.
[15] S.M. Rao, D. Wilton, A.W. Glisson, Electromagnetic scattering by surfaces of arbitrary shape, IEEE Trans. Antennas Propag. 30 (1982) 409–418, http://dx.doi.org/10.1109/TAP.1982.1142818.
[16] A. Taflove, S.C. Hagness, Computational Electrodynamics: The Finite-Difference Time-Domain Method, 3rd edition, Artech House, London, 2005.
[17] S. Makarov, Antenna and EM Modeling with Matlab, 1st edition, Wiley–Interscience, New York, 2002.
[18] K.F. Warnick, W.C. Chew, Error analysis of the moment method, IEEE Antennas Propag. Mag. 46 (2004) 38–53, http://dx.doi.org/10.1109/MAP.2004.1396735.
[19] C.A. Balanis, Antenna Theory: Analysis and Design, 3rd edition, Wiley–Interscience, Hoboken, NJ, 2005.
[20] J. Luo, H. Yu, M. Song, Z. Zhang, Highly efficient wavefront manipulation in terahertz based on plasmonic gradient metasurfaces, Opt. Lett. 39 (2014) 2229–2231, http://dx.doi.org/10.1364/OL.39.002229.
[21] Y. Zhao, A. Alù, Manipulating light polarization with ultrathin plasmonic metasurfaces, Phys. Rev. B 84 (2011) 205428, http://dx.doi.org/10.1103/PhysRevB.84.205428.
[22] N. Yu, F. Capasso, Flat optics with designer metasurfaces, Nat. Mater. 13 (2014) 139–150, http://dx.doi.org/10.1038/nmat3839.
[23] X. Ni, N.K. Emani, A.V. Kildishev, A. Boltasseva, V.M. Shalaev, Broadband light bending with plasmonic nanoantennas, Science 335 (2012) 427, http://dx.doi.org/10.1126/science.1214686.
[24] A. Pors, M.G. Nielsen, R.L. Eriksen, S.I. Bozhevolnyi, Broadband focusing flat mirrors based on plasmonic gradient metasurfaces, Nano Lett. 13 (2013) 829–834, http://dx.doi.org/10.1021/nl304761m.
[25] W.T. Chen, K.-Y. Yang, C.-M. Wang, Y.-W. Huang, G. Sun, I.-D. Chiang, et al., High-efficiency broadband meta-hologram with polarization-controlled dual images, Nano Lett. 14 (2014) 225–230, http://dx.doi.org/10.1021/nl403811d.